New Carbon Materials, 2024, 39(2): 271 - 282

Supporting information

Polyimide-assisted fabrication of highly oriented graphene-based all-carbon foams for enhancing thermal conductivity in polymer composites

XIONG Ke[1], Zhi-peng SUN [1], Ji-chen HU[1], Cheng MA[1], Ji-tong WANG[1,*] Xiang GE[2], Wen-ming QIAO[1,*], Li-cheng LING[1,*]

(1. State Key Laboratory of Chemical Engineering, East China University of Science and Technology, Shanghai 200237, China;

2. Changzhou Fuxi Technology Co, Ltd., Changzhou, 213144, China)

*Correspondence: WANG Ji-tong. E-mail: wangjt@ecust.edu.cn;

QIAO Wen-ming. E-mail: qiaowm@ecust.edu.cn

Received date: ; Revised date:
Corresponding author: WANG Jitong, Professor, E-mail: wangjt@ecust.edu.cn; QIAO Wenming, Professor, E-mail: qiaowm@ecust.edu.cn.

S1 Equations

Bragg's equation

$$d_{002}(\text{nm}) = \frac{n\lambda}{2sin\theta} \quad \text{S1}$$

Mering-Maire equation

$$G(\%) = \frac{0.3440 - d_{(002)}}{0.3440 - 0.3354} \times 100 \quad \text{S2}$$

0.3440: the interlayer spacing of the fully non-graphitized carbon (nm)

0.3354: the interlayer spacing of the ideal graphite crystallite

$d_{(002)}$: the interlayer spacing derived from XRD (nm)

Scherrer equation

$$L_c(\text{nm}) = \frac{K\lambda}{\beta cos\theta} \quad \text{S3}$$

Where λ(nm) is the X-ray wavelength, θ (rad) is the scattering angle, Lc is the average size of the ordered domain, K is a constant, and β is the full width at half maximum (FWHM) of the peak.

Crystalline sizes

$$La = \frac{560}{E_l^4}\left(\frac{I_D}{I_G}\right)^{-1}$$

$$La = \left(2.4\times10^{-10}\right)\lambda^4\left(\frac{I_D}{I_G}\right)^{-1} \quad \text{S4}$$

Where La refers to crystalline sizes. E_l is the excitation laser energy used in the Raman experiment in eV units. λ is wavelength (532nm) of laser in Raman testing.

S2 Figures

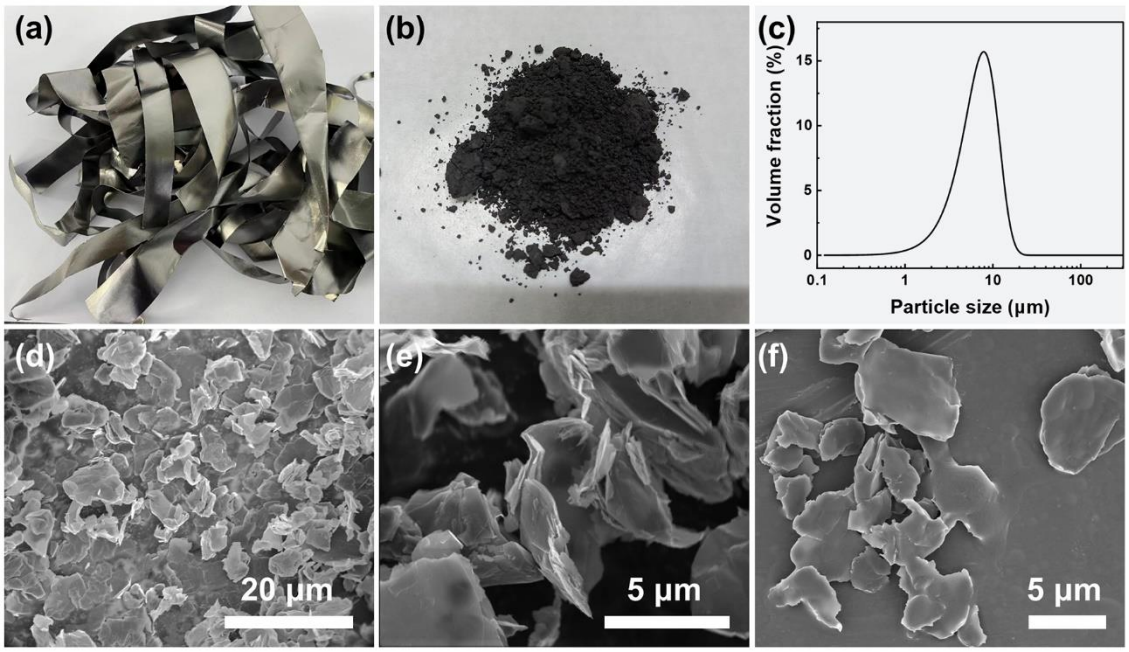

Figure S1. Digital photos of high thermal conductivity graphene film scraps before (a) and after (b) crushing. (c) The particle size distribution curve of GNs. (d-f) SEM images of GNs.

Highly thermally conductive graphene films form a large amount of scraps after the practical cutting and mould cutting process. The GNs were obtained by mechanically and air-flow crushing the high thermally conductive graphene film scraps, with an average lateral size of less than 20 μm, which were manufactured by Changzhou Fuxi Tech Co., Ltd.

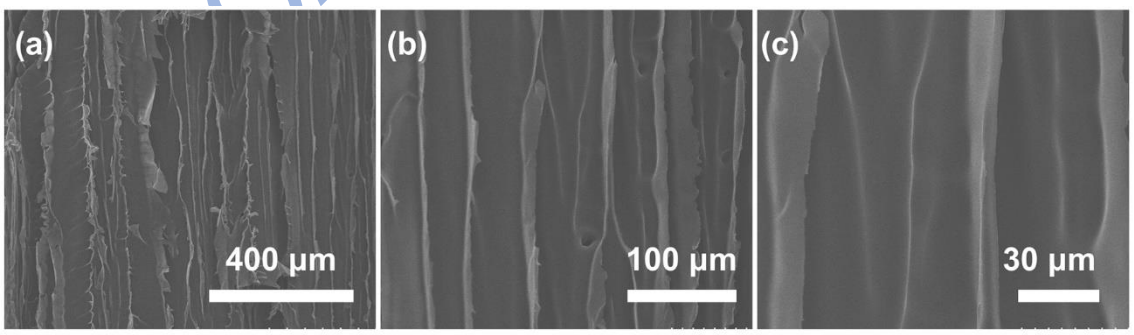

Figure S2. Cross-sectional SEM images of PAA block.

Pure PAA shows a "pea-pod"-shaped array after directional freezing, which effectively assists in the directional alignment of GNs.

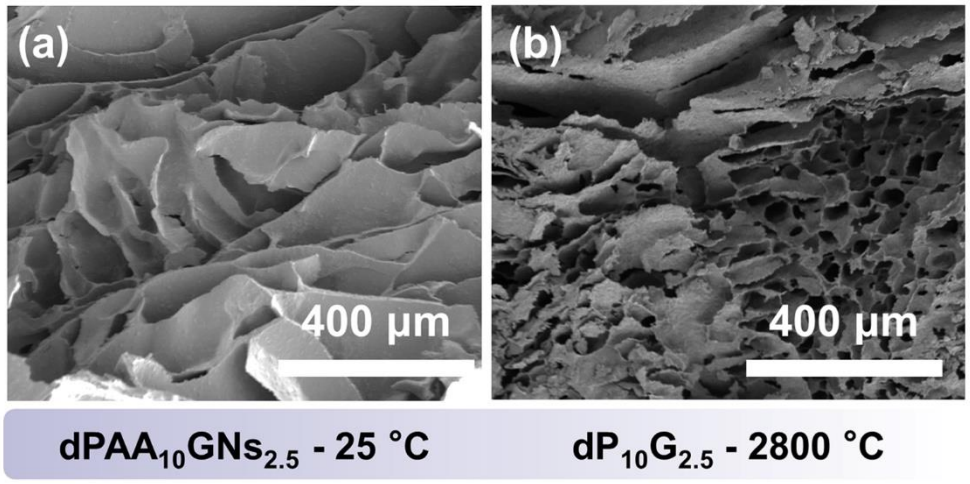

Figure S3. Cross-sectional SEM images of disordered $dP_{10}G_{2.5}$ foam: (a) untreated, (b) graphited.

Compared to the ordered $P_{10}G_{2.5}$ foam, the cross-sectional views of the undirected frozen $dPAA_{10}/GNs_{2.5}$ foam displays a randomly arranged structure, and the disordered networks lead to an increase in the interfacial thermal resistance at the interfaces between the fillers, which retards the heat transfer.

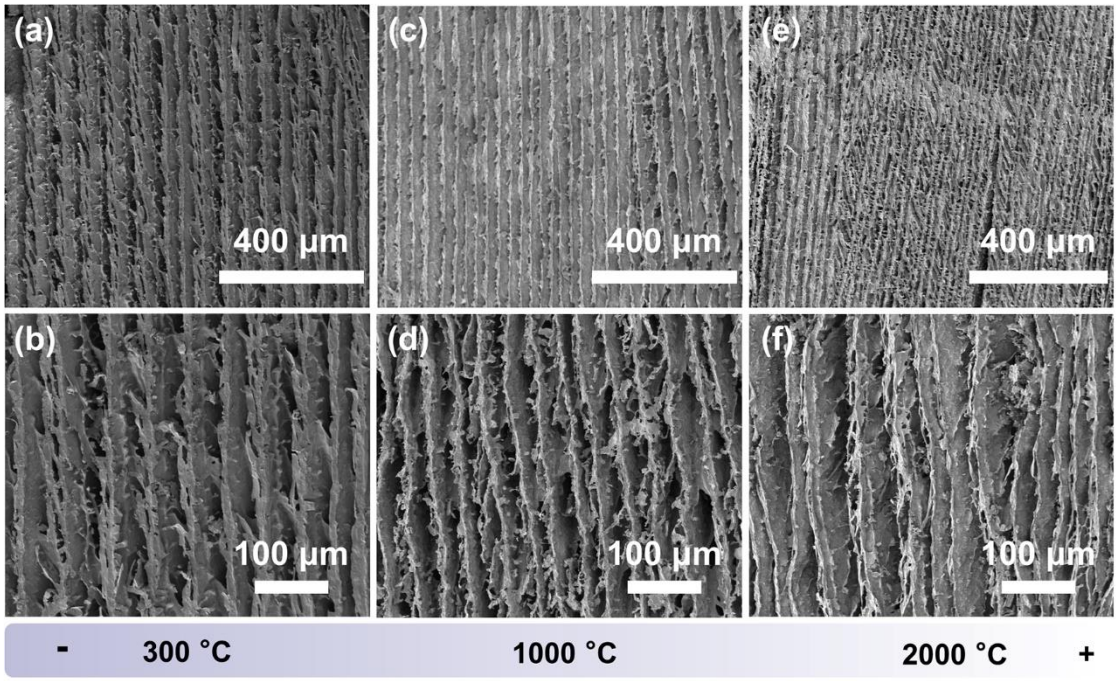

Figure S4. Cross-sectional SEM images of $P_{10}G_{2.5}$ foam at different heat treatment temperatures: (a,b) 300 °C, (c,d) 1000 °C, (e,f) 2000°C.

With increasing annealing temperature in steps, the cross-sectional oriented porous structure of the $P_{10}G_{2.5}$ foam remains complete without significant damage or collapse, maintaining the continuity of the thermal channels.

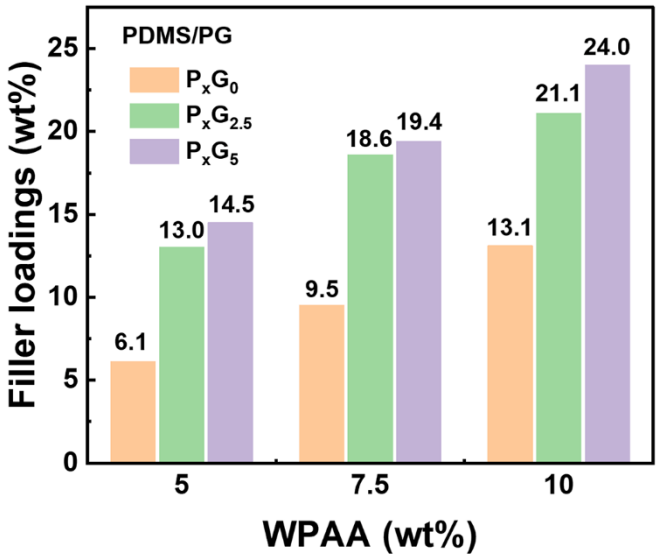

Figure S5. Filler loadings of PDMS/PG composites.

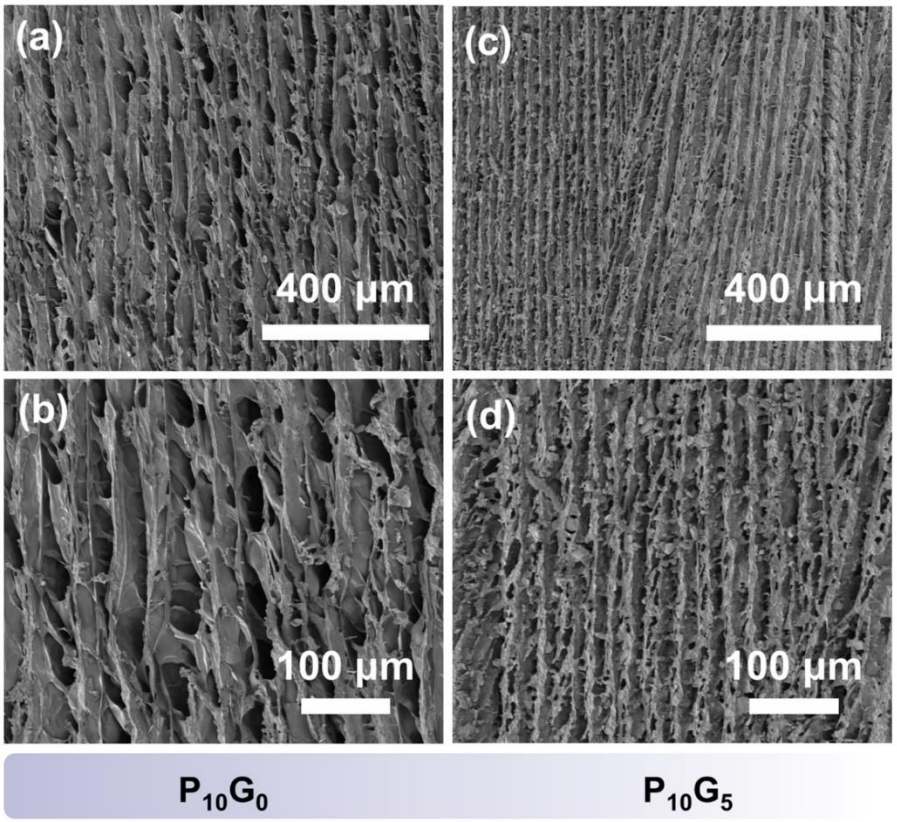

Figure S6. Cross-sectional SEM images of $P_{10}G_y$ foams with different GNs dosage: (a,b) $P_{10}G_0$, (c,d) $P_{10}G_5$.

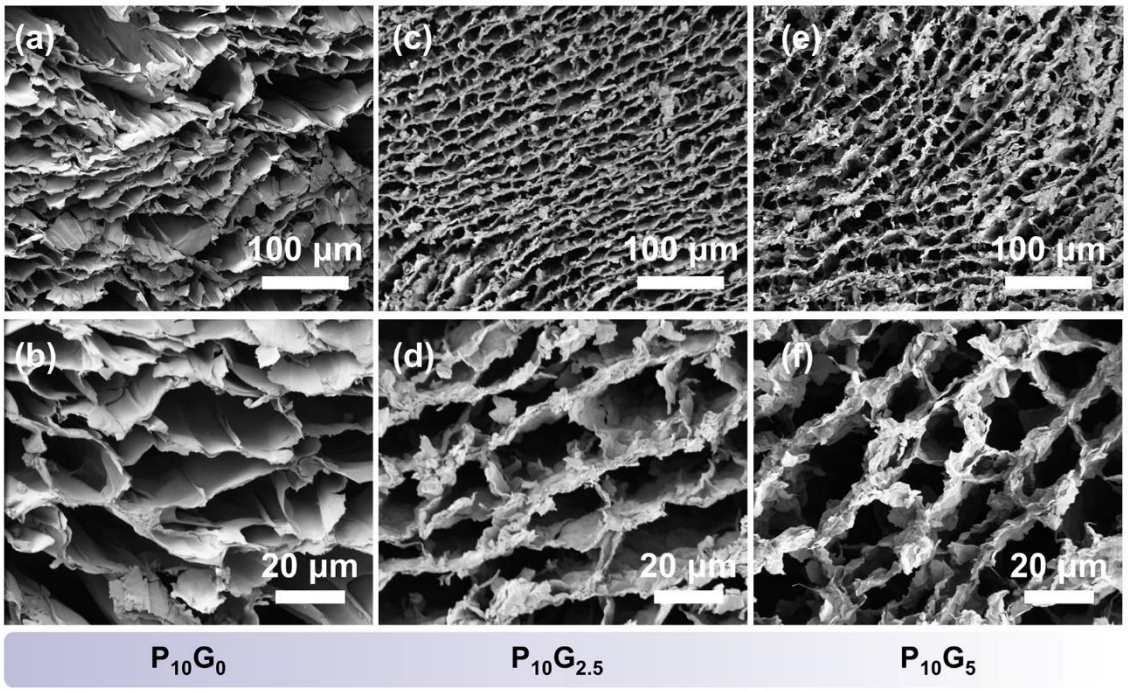

Figure S7. Top view SEM images of $P_{10}G_y$ foams with different GNs dosage: (a,b) $P_{10}G_0$, (c,d) $P_{10}G_{2.5}$, and (e,f) $P_{10}G_5$.

As seen in Figure S5 and Figure S6, $P_{10}G_{2.5}$ is significantly more ordered than $P_{10}G_0$, allowing for more optimal spatial domination of the thermally conductive skeleton. However, excessive GNs result in redundant graphite structures ($P_{10}G_5$).

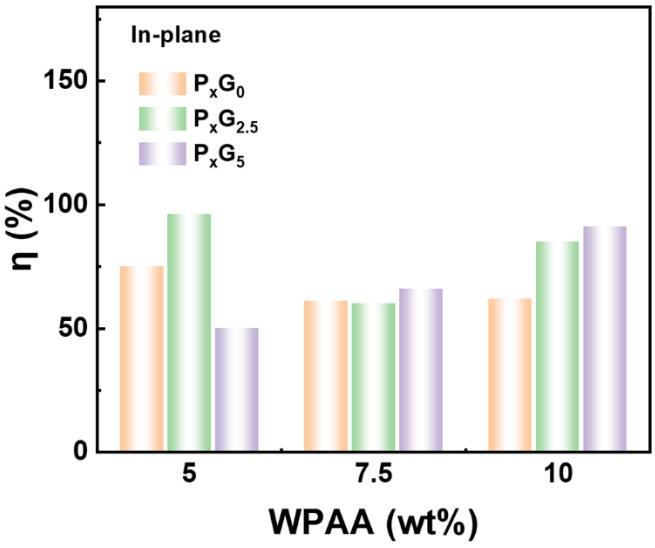

Figure S8. In-plane enhancement efficiency of PDMS/PxGy composites.

For the IP direction, the composites all have η less than 100%, with a value of 85% for PDMS/$P_{10}G_{2.5}$.

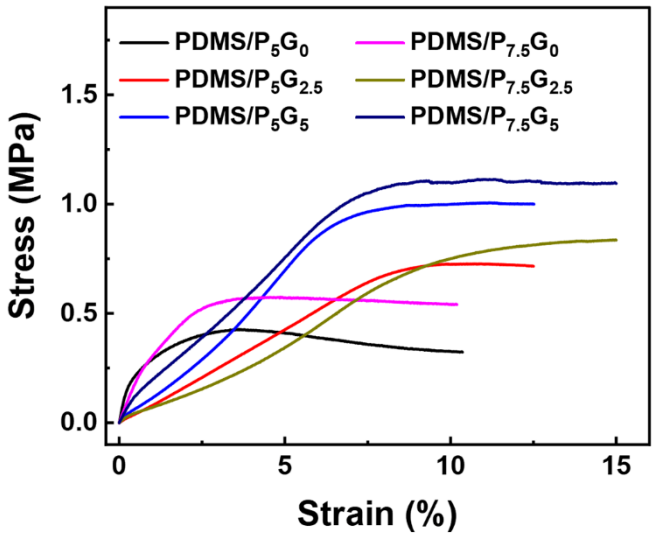

Figure S9. Compressive stress-strain curves of PDMS/PG composites.

Figure S8 describes the compressive stress-strain curves of PDMS/PG composites.

S3 Tables

Table S1. The volume shrinkage and the density of $P_{10}G_{2.5}$.

Sample	$P_{10}G_{2.5}$ Temperature (°C)				
	25	300	1000	2000	2800
Shrinkage ratio (%)	0	30.06	61.54	61.51	61.32
Density ($g \cdot cm^{-3}$)	0.22	0.21	0.25	0.24	0.24

Table S2. The density, porosity, and compressive strength of the PG foams.

Sample	Density ($g \cdot cm^{-3}$)	Porosity (%)	Strength (MPa)
P_5G_0	0.07	96.7	0.05
$P_5G_{2.5}$	0.13	94.3	0.08
P_5G_5	0.16	92.8	0.17
$P_{7.5}G_0$	0.12	94.7	0.16
$P_{7.5}G_{2.5}$	0.20	91.3	0.37
$P_{7.5}G_5$	0.23	89.9	0.60
$P_{10}G_0$	0.16	92.9	0.33
$P_{10}G_{2.5}$	0.24	89.3	0.71
$P_{10}G_5$	0.28	87.6	0.75

Table S3. Structural characterizations of GNs, $P_{10}G_0$ and $P_{10}G_{2.5}$.

Sample	2θ (°)	d_{002} (nm)	Lc (nm)	G (%)	I_D/I_G	La (nm)
GNs	26.53	0.3357	27.28	96.27	0.255	75.39
$P_{10}G_0$	26.28	0.3388	19.22	60.47	0.191	100.65
$P_{10}G_{2.5}$	26.49	0.3362	27.56	90.23	0.232	82.86

The I_D/I_G and La are the average of the Raman mapping areas.